Electrical Characteristics and Modeling of a Filamentary Dielectric Barrier Discharge in Atmospheric Air
(Ciri Elektrik dan Model Suatu Nyahcas Dielektrik Berpenghadang dalam Udara Atmosfera)

W.H. TAY, S.L. YAP & C.S. WONG*

ABSTRACT

The electrical characteristics of a filamentary dielectric barrier discharge (DBD) are studied experimentally and numerically. The DBD system which has parallel plate electrodes geometry is powered by a 50 Hz power supply and operated at atmospheric air. A dynamic electric circuit model considering the discharge region and the non-discharge region being connected by a surface resistance is proposed. Simulation using this model is shown to fit the experimentally measured QV diagram satisfactorily. The effects of the air gap distance and the dielectric surface on the discharge behavior are then investigated. It is found that the surface resistivity of the dielectric is one of the important parameters governing the discharge behavior.

Keywords: Dielectric barrier discharge; electrical characteristics; electrical modeling; filamentary discharge

ABSTRAK

Ciri nyahcas dielektrik berpenghadang (DBD) telah dikaji secara eksperimen dan berangka. Sistem DBD yang mengandungi dua elektrod plat yang selari dikuasakan dengan bekalan kuasa 50 Hz dan beroperasi dalam udara atmosfera. Satu model elektrik yang mengambil kira rantau tidak bernyahcas dan rantau bernyahcas telah dicadangkan. Dalam model elektrik ini, rantau tidak bernyahcas dan rantau bernyahcas disambung dengan satu rintangan permukaan. Keputusan simulasi berjaya menyamai keputusan Lissajous QV yang diperoleh daripada eksperimen. Kesan jarak jurang ruang dan rintangan permukaan dielektrik dalam DBD juga dikaji dan didapati bahawa rintangan permukaan dielektrik adalah satu parameter yang penting untuk mengawal sifat nyahcas.

Kata kunci: Ciri elektrik; nyahcas dielektrik berpenghadang; nyahcas filamen; model elektrik

INTRODUCTION

A dielectric barrier discharge (DBD) is produced when at least one of the electrodes of a gas discharge powered by an alternating or pulsed current source is covered by dielectric. The dielectric barrier discharge has been the subject of extensive research by many researchers recently because of its simplicity in operation and yet with great potential in industrial applications. Nowadays the dielectric barrier discharge is being considered for applications such as ozone synthesis (Ramasamy et al. 2001; Subedi et al. 2012), removal of toxic gases (Hashim et al. 2007, 2010), surface treatment of materials (Wagner et al. 2003) and generally as a chemical reactor for a large variety of reactions (Kogelschatz et al. 1999; Kogelschatz 2002, 2003).

The dielectric barrier discharge is most commonly generated in the filamentary mode when operated at atmospheric pressure. A large number of individual channels (filaments) each with millimeter size diameter and nanoseconds duration are observed to be randomly distributed within the discharge gap (Kogelschatz 2002, 2003). The electric field across the discharge gap is built up by charge accumulation at the dielectric surface until quench discharge occurs (Kogelschatz 2002, 2003). The

next ignition of DBD's discharge channel will occur after sufficient electric field is built up again. The ignition and quenching processes leading to the formation of the discharge channels are repeated at both the positive and negative peaks of the applied alternating voltage. With applied voltage of higher amplitude, more discharge channels can be generated. The larger number of discharge channels may be caused by the resistivity or charge trapping property of the dielectric surface. Hence, the accumulations of charges do not spread out uniformly on the dielectric surface but instead they are deposited as residual charges on the dielectric surface. After the reversal of polarity of the applied voltage, the accumulation of charges on the dielectric surface which support non-homogeneous electric field leads to the formation of DBD channels at the same location as those occurred during the previous half cycle. This is referred to as the memory effect.

Under certain selected operating conditions, dielectric barrier discharge in a homogenous mode can be observed (Brandenburg et al. 2009; Kogelschatz 2003). A dynamic electrical model for homogeneous discharge has been put forward by Liu and Neiger (2003). However, the electrical properties of a filamentary discharge are more complicated due to the presence of collective phenomenon.

For filamentary mode, the microdischarge is distributed randomly across the dielectric surface. It consists of numerous discharge channels separated from each other. On the other hand, for a homogenous Townsend discharge, a single discharge is observed to cover the entire discharge region (Gherardi & Massines 2001).

Bhosle et al. (2004, 2005) considered a discrete number of microdischarges by introducing an electrical model consisting of multi filaments, each correlate to one micro discharge. A single filament in the model is represented by a time dependent conductor and ignited by a TRIAC switch controlled by the voltage across the space gap. In another work, a filamentary discharge has been modeled by employing a high frequency sinusoidal generator in an analog electrical circuit (Valdivia-Barrientos et al. 2006).

The purpose of this work was to investigate the electrical characteristics of the DBD in the filamentary mode. An electrical model has been proposed to simulate the observed electrical characteristics of the DBD. In the discharge circuit model proposed here, the space gap discharge region is represented by a resistive current and a capacitor connected in parallel, while the non-discharge region is represented by a single capacitive current. These two currents are connected by a surface resistance due to the presence of the dielectric.

EXPERIMENTAL DETAILS

The experimental setup is shown schematically in Figure 1. The DBD used has a parallel-plate electrodes geometry. Two circular stainless steel plate electrodes with diameter of 60 mm are separated by a glass plate with thickness of 2.0 mm and an air gap. The air gap distance is variable in the range of 0.2 to 5.0 mm. The location of the dielectric with respect to the electrodes can be varied. The upper electrode is connected to the high voltage through a ballast resistor R_1 of 8.8 MΩ. The DBD system is powered by a 50 Hz power supply and the maximum voltage available is 40 kV (peak-to peak value). The bottom electrode is connected to a single pole double throw (SPDT) switch which is connected to a resistor R_2 (100Ω) and a capacitor C_1 (0.47μF) in parallel.

The top electrode is a copper ring coupled to a piece of transparent conductive layer, Indium tin oxide (ITO) for the experiment to determine the ratio of the discharging regions to the non-discharging regions. The image of the DBD discharge has been captured from the top view of the DBD reactor through the ITO using a high-speed intensified charge-coupled device (ICCD) camera.

The discharge current is monitored across the resistor R_2 (100Ω) and the capacitor C_1 (0.47μF) is used to monitor charge transfer. The voltage across R_2 or C_1 is measured by a 10 times voltage probe and the voltage of the upper electrode is measured by a 1000 times high voltage probe. Both voltages are recorded simultaneously by a Tektronix TDS2024 oscilloscope with a bandwidth of 200 MHz and a sampling rate of 2 GS/s. This system is operated at atmospheric pressure either with air or an admixture of nitrogen and oxygen. The signals of the discharge current and voltage for the filamentary DBD discharge are shown in Figure 2(a). The single discharge pulse signal in high time resolution is recorded by digital Yogokawa DL6104 oscilloscope with a bandwidth of 1 GHz as shown in Figure 2(b). If the amplitude of space voltage is above the breakdown voltage, large number of discharge current pulses will be observed. The discharge pulses are observed to be generated during the rising edge of the current pulse, which is labeled as breakdown period. For simplicity, we
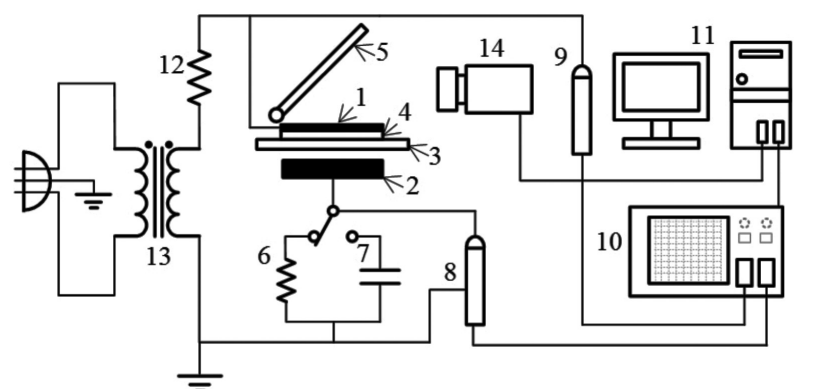
1.	Ring shape electrode	8.	10 times voltage probe
2.	Ground electrode	9.	High voltage probe
3.	Dielectric sheet	10.	Tektronic TDS2024 oscilloscope
4.	ITO	11.	Computer interfacing
5.	Mirror	12.	Ballast resistor, R1
6.	Current monitor resistor, R2	13.	HV Transformer
7.	Charge monitor capacitor, C1	14.	ICCD Camera

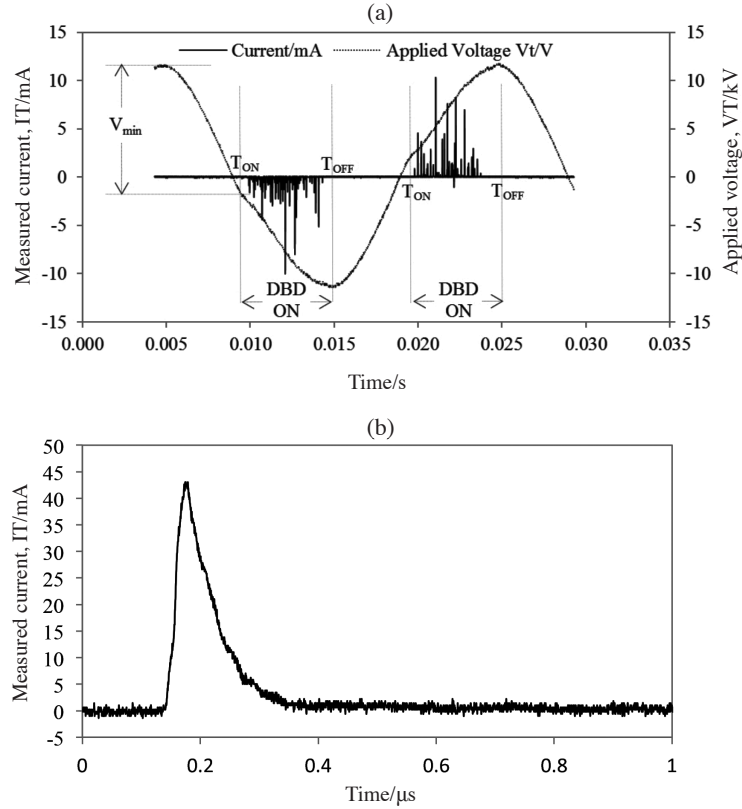FIGURE 1. Schematic diagram of the experimental setup

FIGURE 2. (a) A sample of DBD discharge current spikes and applied voltage. V_{min} is pk-pk minimum breakdown voltage. The DBD is 'ON' during the time period from T_{ON} to T_{OFF}. (b) A sample of single discharge pulse in high time resolution

denote breakdown period and non-breakdown period as 'ON' period and 'OFF' period, respectively. The DBD ON period is the period from the ignition time, T_{on} until the cessation time, T_{off}.

For the measurement of the equivalent capacitance of the discharge gap before breakdown (C_T), the switch in Figure 1 is connected to capacitor C_1. The capacitor C_1 with a much higher value than C_T is selected to minimize its effect on the overall circuit. The measured voltage of capacitor C_1 is divided by the capacitance value (0.47 μF) to give the total charge transfer. For this measurement, the applied voltage is kept below the breakdown voltage. The total charge transfer versus applied voltage is then plotted and a single straight line is obtained. From the slope of this plot, the equivalent capacitance (C_T) is determined. Apart from this, the space gap capacitance is calculated using the expression:

$$C_g = \frac{S \in_r \in_o}{d}, \tag{1}$$

where d is the distance of space gap, $\in_r$ is the relative permittivity of air space which is approximated to 1, and $\in_o$ is the vacuum permittivity. Due to the thickness of the electrode 1.5 cm, the electrode edge effect on the space gap capacitance cannot be ignored. The area, S is the summation of the actual electrode area and the edge

area. The magnitude of the edge capacitance is directly proportional to the perimeter of electrode (Kamchouchi & Zaky 1975). For the present experimental setup, the effective edge distance is approximately 1 mm from the boundary of the electrode for small space gap. The actual electrode radius is 30 mm. The edge effect is assumed to be not affected by the DBD discharge due to high surface resistivity of glass plate.

The value of space capacitance (C_g) obtained from the calculation is utilized to determine the total dielectric capacitance (C_d) from (2). C_T is equal to the slope of linear plot of the QV diagram.

$$C_d = \frac{C_g C_T}{C_g - C_T}. \tag{2}$$

The experimental values of C_T, C_g and C_d are important parameters required for the electrical modeling.

For the breakdown voltage measurement, the QV diagrams of different applied voltages are plotted and the breakdown voltage of DBD can be determined from the QV diagram by using the Manley's method (Manley 1943). The experimental dissipation energy per cycle is also determined by the area under the QV diagram as given by (3).

$$E = \oint V(t) \, dQ. \tag{3}$$

However, the surface dissipation energy and the surface resistance of the dielectric are not measurable directly from the experiment. They can be determined by fitting the simulated QV diagram to the experimentally measured QV diagram.

EQUIVALENT CIRCUIT FOR THE DBD

By employing Manley's method (Manley 1943), the space gap voltage V_g can be considered as constant ignition voltage during a discharge period. If the surface current is ignored, the total discharge current is equal to the total current passing through the DBD system while the space gap voltage is maintained at a constant value during the total discharge period.

The Manley's method has been shown to be able to successfully explain filamentary discharges produced in certain range of conditions. However, in the case of a low frequency discharge such as 50 Hz and high resistivity dielectric surface, the voltage observed across the air gap actually increases during the discharge. This effect is believed to be due to a resistance to the charge flow on the dielectric surface and non-uniform breakdown channel. Therefore, V_g is no more constant. This is obvious from the experimental observation, where the breakdown voltage V_b determined from QV diagram increases with increased applied voltage. The slope of QV diagram also changes with increased voltage showing significant expansion of the width of QV diagram. This observation is also observed and studied by Kim et al. (2006). Their model is based on the explanation given by Kozlov et al. (2001). According to Kozlov et al. (2001), the cathode fall layer is stabilized between the space gap during the discharge. This cathode fall layer is considered as a variable virtual capacitor. But for filamentary discharge, the cathode fall layer is unable to achieve stability within the nanosecond discharge duration.

In this work, we propose a dynamic electrical circuit model where the effect of the dielectric surface resistivity has been taken into consideration.

The proposed model is similar to the one proposed by Bhosle et al. (2004). In the present proposed model we have included surface discharge and the interaction of filament discharges with each other. The electrode region has been divided into discharge region and non-discharge region as shown on Figure 3. The discharge filaments are assumed to be generated at the same locations due to the memory effect (Chirokov et al. 2006). The lifetime of each discharge filament is about a few nanoseconds (Kogelschatz et al. 1997) and the sum of all the discharge channels is considered to be the discharge region in our model.

Applying the similar concept as Bhosle et al. (2004), a coefficient D is introduced which is equal to the ratio of the total discharge region to the total electrode area. Hence, we get:

$$D = \frac{\sum S_D}{S}, \tag{4}$$

where S is the total electrode area. S_D is the effective area of an individual filament discharge. The factor D has been first obtained experimentally through the imaging of the DBD. The image captured is shown in Figure 4. There are regions consistently bright indicating the discharge regions. The regions consistently dark are indicating the non-discharge regions.

The capacitance of the DBD system is assumed to be consisting of 2 components, one being contributed by the discharge region ($C_{d,D}$) while another contributed by the non-discharge region ($C_{d,N}$). This allows us to study the dynamic electrical behavior of the discharge and the interaction of the current channels with each other. The capacitance C_d represents the total capacitance of the dielectric covering the total electrode area and it is given by:

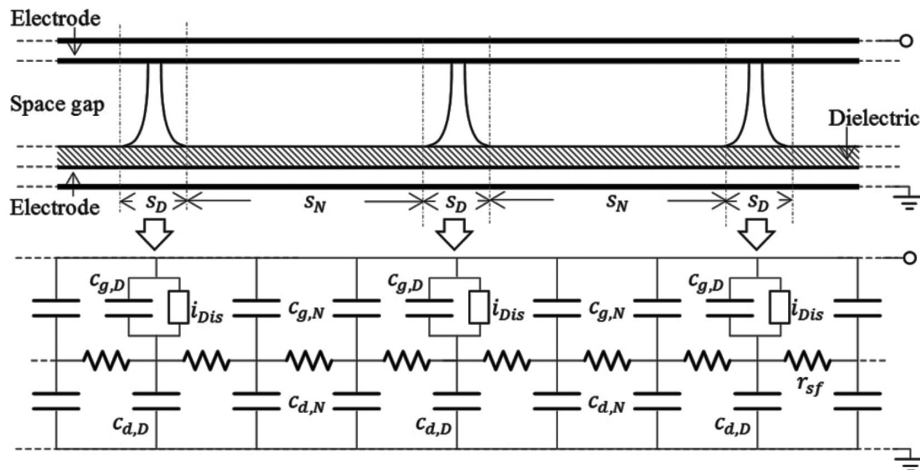$$C_d = \left(\sum S_D + \sum S_N\right)\frac{\in_r \in_o}{d_T}, \tag{5}$$

FIGURE 3. The schematic diagram showing the non-discharge region, S_N and discharge region, S_D represented in the electrical circuit
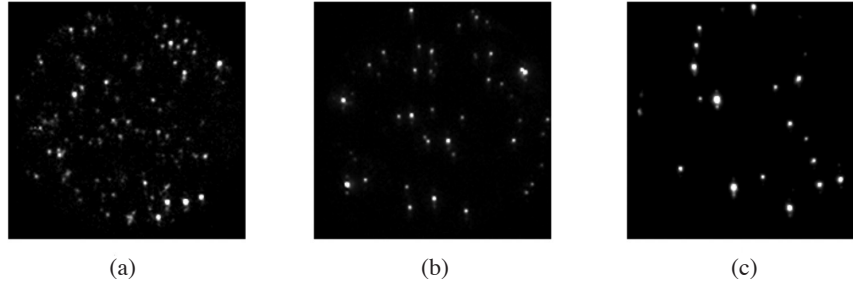
FIGURE 4. The top view of the DBD reactor operated with (a) 0.2 mm space gap,
(b) 0.5 mm space gap and (c) 1.0 mm space gap

where d_T is the thickness of dielectric layer, $\in_r$ is the relative permittivity of the space (taken to be 1 for air), $\in_o$ is the vacuum permittivity, $\Sigma\,S_N$ is the total area of the non-discharge region, while $\Sigma\,S_D$ is the total area of the discharge region.

Equation (5) can also be written in the form,

$$C_d = C_{d,D} + C_{d,N}. \tag{6}$$

Rearranged, the equation is written in the form,

$$C_{d,D} = DC_d. \tag{7}$$

$$C_{d,N} = (1-D)\,C_d. \tag{8}$$

Similarly, the total space capacitance, C_g is also composed of the discharge and non-discharge regions, which gives:

$$C_g = C_{g,D} + C_{g,N}. \tag{9}$$

$$C_{g,D} = DC_g. \tag{10}$$

$$C_{g,N} = (1-D)C_g. \tag{11}$$

The important parameters such as $C_{d,D}, C_{d,N}, C_{g,D}$ and $C_{g,N}$ are not measurable directly. Therefore, these values are estimated using experimentally measurable values such as C_d and C_g.

For filamentary discharge, each current source represents a single discharge channel and the discharge channels are connected with each other by surface resistance across the non-discharge regions. The surface properties or the trapped charges (Li et al. 2008) on the dielectric surface have important influence on the discharge behavior. A potential difference on the dielectric surface was observed by Bartnikas et al. (2007) and it was attributed to the high surface resistivity of the dielectric. It can be associated with the accumulated charges on the dielectric surface. If the surface resistivity is too small and the power system is operated at low frequency, the surface charges may spread due to ohmic conduction and the spreading charges may distort the space gap electric field

in the region surrounding it (Somerville & Vidaud 1985). In order to simplify the electrical circuit model, all the discharge channels and the immediate regions surrounding them are lumped together to form the discharge region while the regions which are far from the discharge channels are clumped together to form the non-discharge region. The non-discharge region and the discharge region are connected with a surface resistance.

The simplified equivalent circuit of the proposed lumped discharge model for the DBD is shown in Figure 5. This equivalent electrical circuit consists of three parallel lines of current flow. The discharge region and the non-discharge region are represented by two capacitors in series. The third line consists a single capacitor, C_s which is the stray capacitance due to cable and/or edge effect (Falkenstein & Coogan 1997). The discharge through the space gap is represented by a voltage control current source. The discharge region and the non-discharge region are assumed to be connected by a resistor with a fixed value of R_{sf}, which is related to the surface resistive effect of the dielectric.

V_g, V_d and V_T represent the average voltages between the space gap, the dielectric and the electrodes, respectively. The average values of V_g, V_d and V_T can be determined from the experimental results. In this proposed model, these voltages are divided into the discharge region voltages ($V_{g,N}, V_{d,N}$ and $V_{T,N}$) and the non-discharge region voltages ($V_{g,D}, V_{d,D}$ and $V_{T,D}$) as shown in Figure 5. These voltages cannot be measured directly from the experiment.

Before breakdown, the capacitive displacement current due to the time-varying applied voltage is flowing through the electrodes uniformly. The DBD's system is acting as a pure capacitor. This gives rise to a straight line in the QV diagram. In this proposed model, before DBD breakdown the discharge current source is not activated. The general equation of dielectric voltage calculation is given by Liu and Neiger (2003) and Pal et al. (2009) as:

$$V_d(t) = V_d(0) + \frac{1}{C_d}\int_0^t I_T(t)dt, \tag{12}$$

where $V_d(0)$ is to obtain the initial dielectric voltage. For the experimental results the integrated current can be obtained from the total charge transfer measured by charge monitor capacitor C_1. The experimental total charge
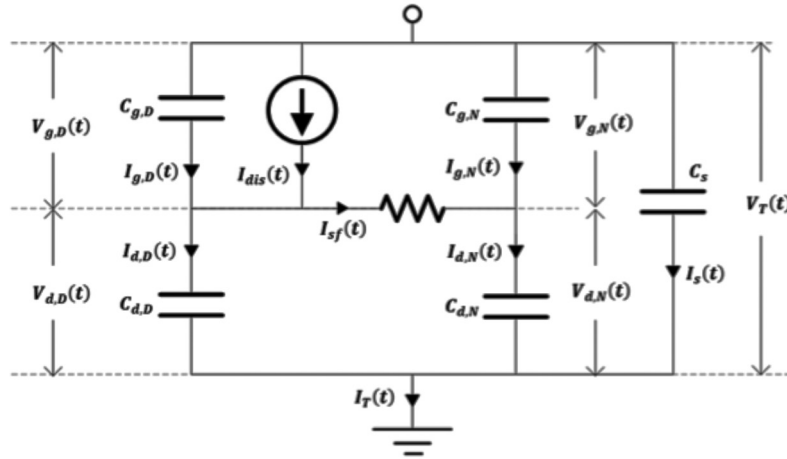
FIGURE 5. The equivalent electrical circuit of DBD indicating the discharge currents

transfer is utilized to determine the average dielectric voltage.

The value of dielectric voltage, $V_d(t)$ is utilized to calculate the space gap voltage.

$$V_g(t) = V_T(t) - V_d(t). \tag{13}$$

These general equations are available for both conditions (before breakdown and after breakdown).

The total effective discharge time in the discharge region is very short due to the short duration of individual discharge pulse. Hence, the space gap capacitance of the discharge region is assumed to be constant through the total duration of the DBD. After breakdown, the DBD discharge current source which is assumed to be voltage controlled (Flores-Fuentes et al. 2009; Naude et al. 2005), generates a discharge current, $I_{dis}(t)$ given by:

$$I_{dis}(t) = I_o \left(\frac{V_{g,D}(t)}{V_{nb}} \right)^{\alpha}. \tag{14}$$

The discharge current is strongly dependent on the space voltage of the discharge region. Here is the breakdown voltage which a constant value. The values of α and I_o are dependent on the operating condition. This approach has been used by Flores-Fuentes et al. (2009) in their electrical model. This expression can be used to estimate the average current during the transition from the non-discharge to discharge condition. The values of α and I_o are adjusted to match the computed QV diagram to the experimentally measured QV diagram. The slope of the experimental QV diagram is changing with the applied voltage during the transition. The change of QV slope is large and cannot be fitted by any reasonable values of α and I_o if without considering the surface resistance effect. The generated discharge current is flowing through the discharge region. The deposited charges for both the space gap and dielectric in the discharge region induce a potential difference between the discharge region and

the non-discharge region. This potential difference can be explained by the presence of a resistance between them on the surface of the dielectric. The current flowing through the surface path between the discharge region and the non-discharge region can be written as:

$$I_{sf}(t) = \frac{V_{d,D}(t) - V_{d,N}(t)}{R_{sf}}, \tag{15}$$

where R_{sf} is the total effective resistance between the discharge and non-discharge regions on the dielectric surface.

The total energy (E_{Total}) calculated from the experimentally measured QV diagram is the sum of energy dissipated on the surface ($E_{surface}$) and the DBD discharge (E_{DBD}). The total dissipation energy of the DBD in one cycle is given by:

$$E_{Total} = \int_0^T V_T(t) I_T(t) dt. \tag{16}$$

The energy consumed by the surface resistance in one cycle is:

$$E_{surface} = \int_0^T \frac{\left(V_{d,D}(t) - V_{d,N}(t)\right)^2}{R_{sf}} dt. \tag{17}$$

And the energy of the DBD discharge in one cycle is:

$$E_{DBD} = \int_0^T V_{g,D}(t) I_{dis}(t) dt. \tag{18}$$

MATLAB SIMULINK CODE

The dynamic circuit model proposed in this work which consists of the discharging region and the non-discharging region has been implemented by using Matlab Simulink. The arrangement of the circuit elements in Simulink code is shown in Figure 6. An AC voltage source at 50 Hz is

employed as the power source, where the inductance of the power transformer is ignored. The outputs from the simulation of the dynamic circuit are given by plotting the current and voltage signals of the discharge.

In the circuit elements in Simulink code, the discharge current is generated by a voltage control current source. The Simulink code of the voltage control current source is shown in Figure 7(a). The voltage across the IN and OUT of the voltage measurement block represents the space gap voltage of the discharge region, which is $V_{g,D}$.

Other measurable and computable quantities to be compared included the dissipated power, voltage across
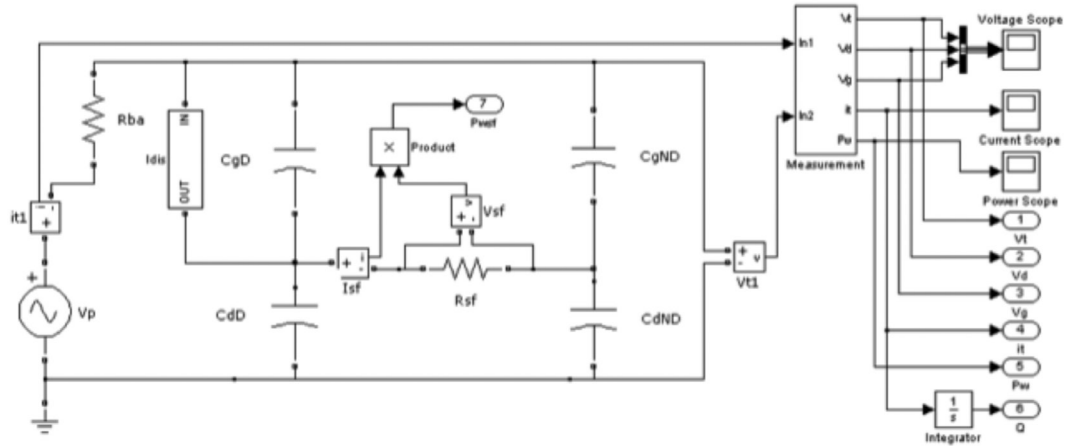
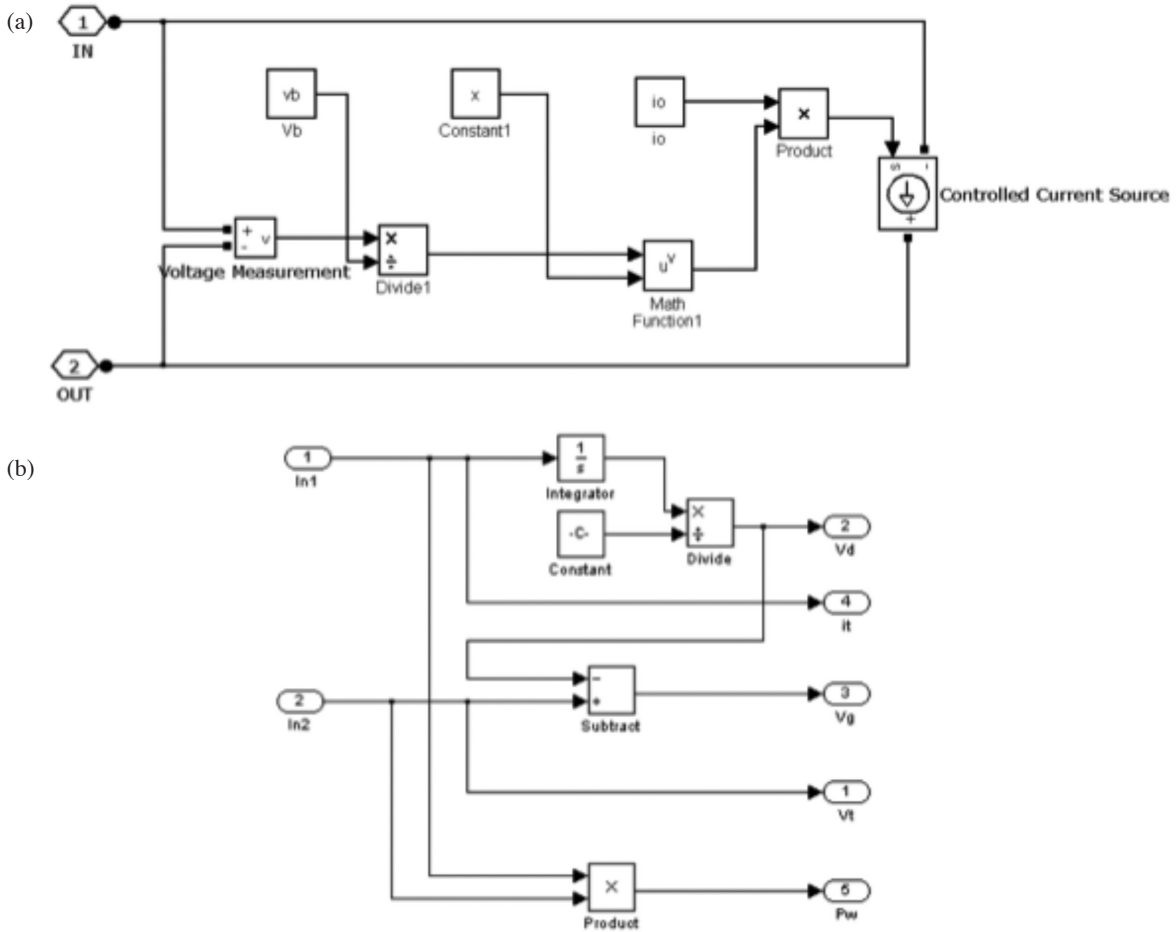FIGURE 6. The interface of Matlab simulink code

FIGURE 7. The Simulink code of (a) discharge current blocks and (b) measurement and analysis block

the space gap and voltage across the dielectric. Hence, in order to obtain the QV diagram, space gap voltage and the dissipation power from Matlab Simulink, the current and voltage signals registered in Matlab Simulink has been analyzed by sending them to the analysis block via input IN1 and IN2, respectively, as shown in Figure 7(b).

The total voltage across the DBD cell and the equivalent current that have been measured experimentally can be compared with the simulated output. By employing (16), (17) and (18), the calculated energies from the simulation results are also compared with the experimental results.

EXPERIMENTAL AND SIMULATION RESULTS

A typical set of experimental results and simulated results are presented in Figure 8 for DBD with 0.5 mm air gap and 30 kV applied voltage. The values of the average dielectric voltage V_d and discharge gap voltage V_a which are not measureable experimentally are calculated using (12) and (13), respectively. The simulated results agreed very well with the experimental results as shown in Figure 9.

Rate of change of the charge transfer measured across capacitor C_1 (Figure 1) gives the average total currents. The dissipated power of the air gap can be obtained by multiplying the average total current and the voltage of the air gap. Both calculated total gap power and total current from simulation results and experiments are shown in Figure 10 for discharge with 0.5 mm air gap and 30 kV peak-to-peak applied voltage. As can be seen from Figure 10, there exists a close agreement between the experimental results and the simulated results.

The simulated results were used to plot a QV diagram and compared to the obtained results experimentally. In order to fit the QV diagram plotted from the experimental results, a suitable value of surface resistance R_{sf} has to be assumed.

The value of the surface resistance is correlated to the surface roughness of the dielectric layer. Thus two types of glass plates were investigated; one of rough surface and the other one of smooth surface.

For the DBD with 0.2 mm air gap, with smooth glass plate as the dielectric layer, suitable value of surface resistance was found to be 2.1 MΩ for all the applied voltages. The QV diagrams obtained from the simulation are found to be in almost perfect match with the obtained results experimentally for all the applied voltages from 10 to 35 kV (Figure 11). When the air gap is increased to 0.5 and 1.0 mm, the effective surface resistances required are found to be 2.3 and 1.0 MΩ, respectively. The results for 0.2 and 0.5 mm air gap are considered to be almost the same, but the surface resistance for the case of 1.0 mm is significantly reduced. The results for 1.0 mm air gap are shown in Figure 12. This observation suggests that the effective surface resistance is also affected by the thickness of the air gap.

A careful inspection of the experimental QV diagram has shown significant expansion when the applied voltage was increased from 10 to 35 kV. The area covered by the QV diagram represents the energy dissipated to the DBD at that applied voltage. The expansion shows that the energy dissipated is higher than what is predicted by Manley's equation (Manley 1943). The expanded QV diagrams have been accurately matched by the simulation using our model. The additional energy dissipated is believed to be related to the surface resistance where the energy has been consumed during the charge transfer from the discharging region to the non-discharging region through the surface resistance. Thus the introduction of the surface resistance in our model has allowed us to estimate the total energy dissipated during the DBD accurately.

In order to further clarify the effect of the surface resistance with relation to the surface properties of the dielectric, the results obtained for discharges using smooth glass plate were compared with that using rough glass plate. The experiment with air gap of 1.0 mm is repeated replacing the smooth glass plate with the rough glass plate for the same applied voltage from 10 to 35 kV. The surface resistances obtained when rough glass plate is used as the
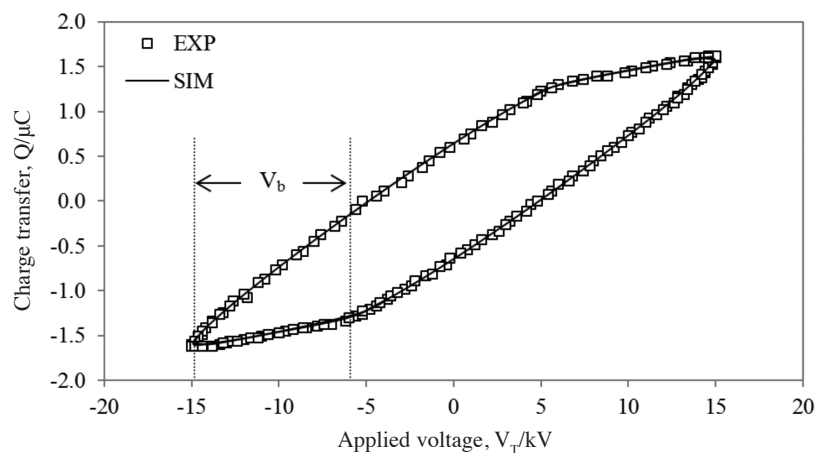

FIGURE 8. A typical QV diagram resulting from (a) simulation and (b) experiment with 0.5 mm air gap and applied voltage of 30 kV pk-pk with values of coefficient D and surface resistance 0.014 and 2.3 MΩ, respectively

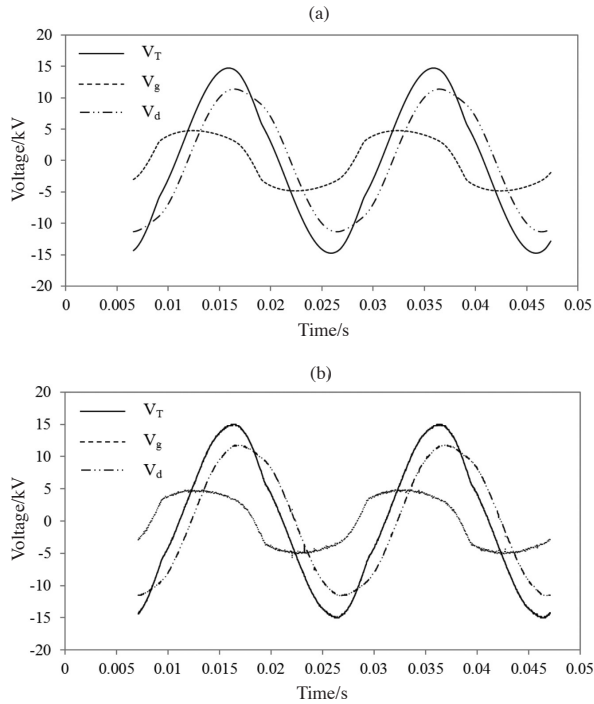FIGURE 9. Comparison of (a) simulated and (b) experimental values of the applied voltage V_T, space gap voltage V_g, and dielectric voltage V_d for 0.5 mm air gap and 30 kV pk-pk applied voltage
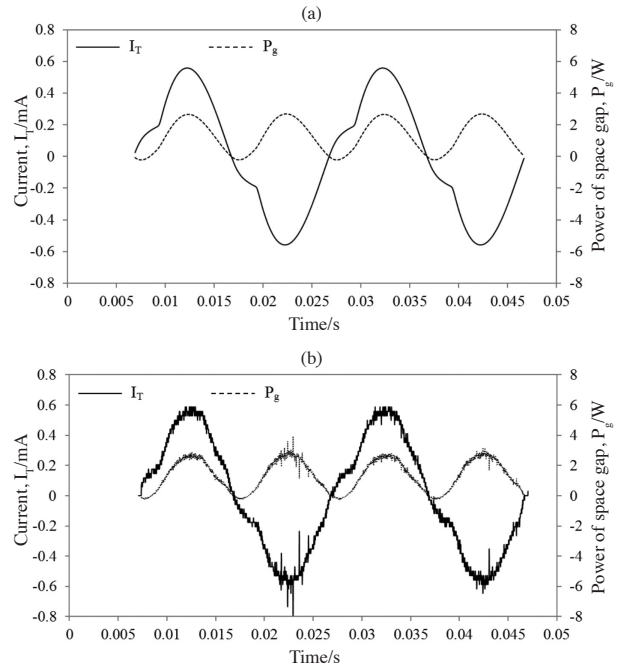

FIGURE 10. Comparison of (a) simulated and (b) experimental values of the dissipation power of space gap (dotted line) and whole discharge (black line) with 0.5 mm space gap and 30 kV pk-pk applied voltage
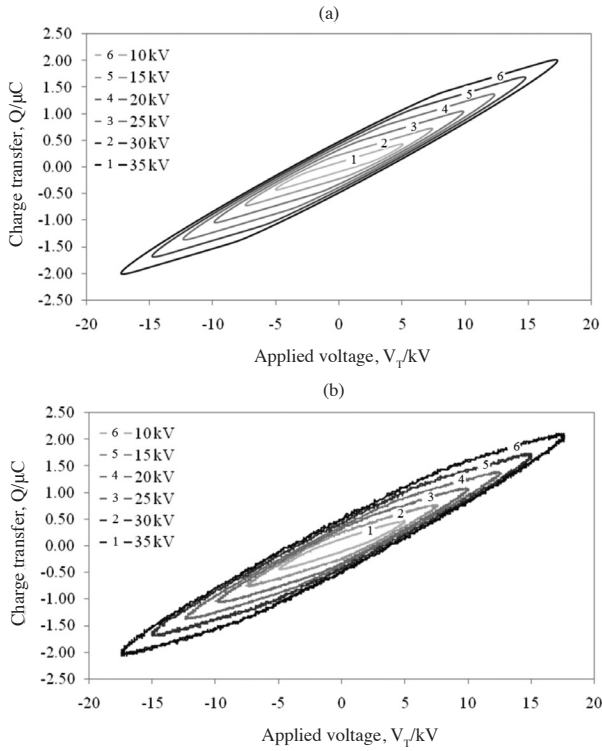

FIGURE 11. QV diagrams resulting from (a) simulation and (b) experiment with 0.2 mm air gap and various applied voltages. The coefficient D and surface resistance used are 0.013 and 2.1 MΩ, respectively
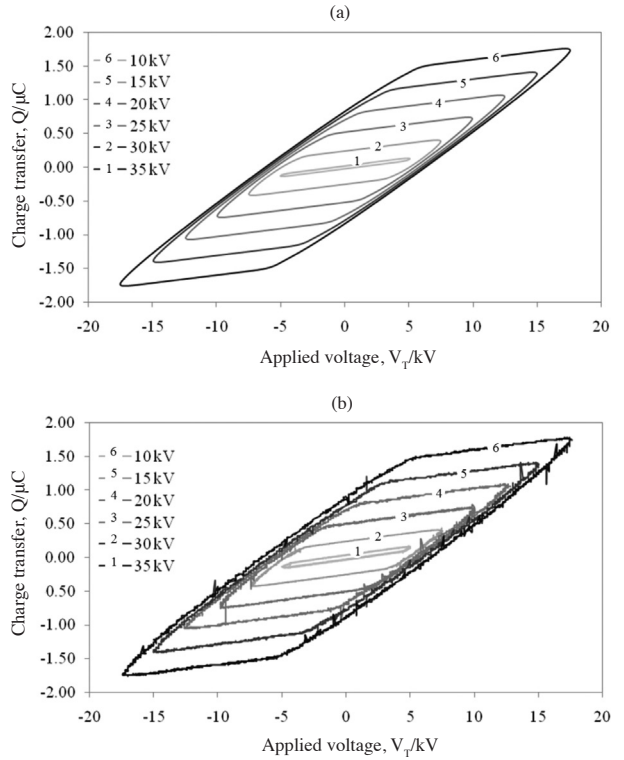

FIGURE 12. QV diagrams resulting from (a) simulation and (b) experiment with 1.0 mm air gap and various applied voltages. The coefficient D and surface resistance used are 0.017 and 1.0 MΩ, respectively

dielectric layer were significantly higher, at a value of 4.5 MΩ. Figure 13 shows the QV diagrams obtained from simulation with surface resistance of 4.5 MΩ for air gap of 1.0 mm. The results agree well with the experimental results for all the applied voltages.

The total energy consumed in the DBD for one complete cycle can be calculated based on (16) or determined from the area under the QV diagram. The values obtained from the QV diagram based on experimental data are plotted for

all the applied voltages and thickness of gaps as shown in Figure 14 (marked by various symbols). The simulated values are also plotted in the same figure for comparison. The experimental points are found to agree well with the simulation. The results obtained from the model for all the experimental parameters are summarized in Table 1.

The total capacitance as measured from the gradient of QV diagram remains the same with different applied voltages at consecutive cycles. This indicated that during
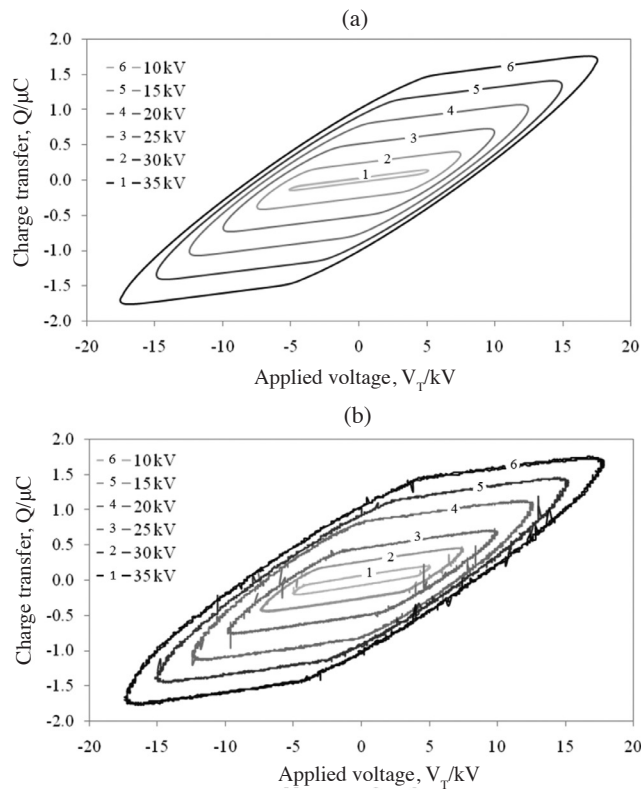

FIGURE 13. QV diagram resulting from (a) simulation and (b) experiment with 1.0 mm air gap and various applied voltages. The coefficient D and surface resistance used are 0.017 and 4.5 MΩ, respectively
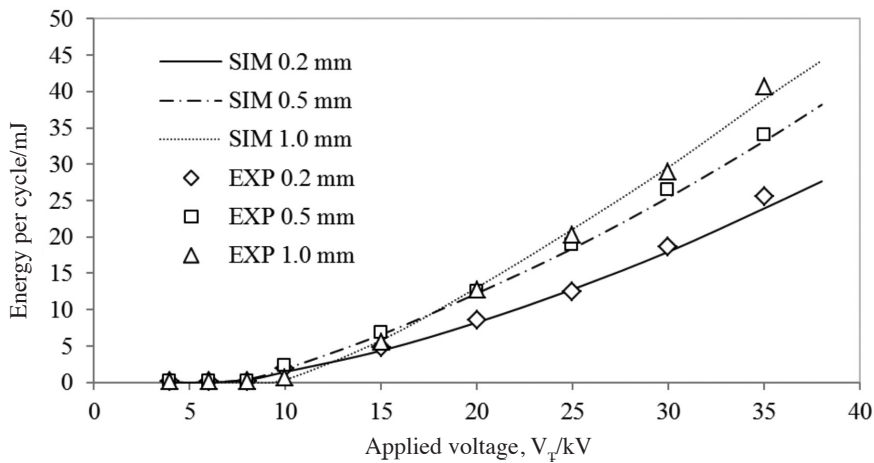

FIGURE 14. The graphs of total energy versus applied voltage with various air gaps. The lines represent the simulated results and the symbols are representing the experimental results
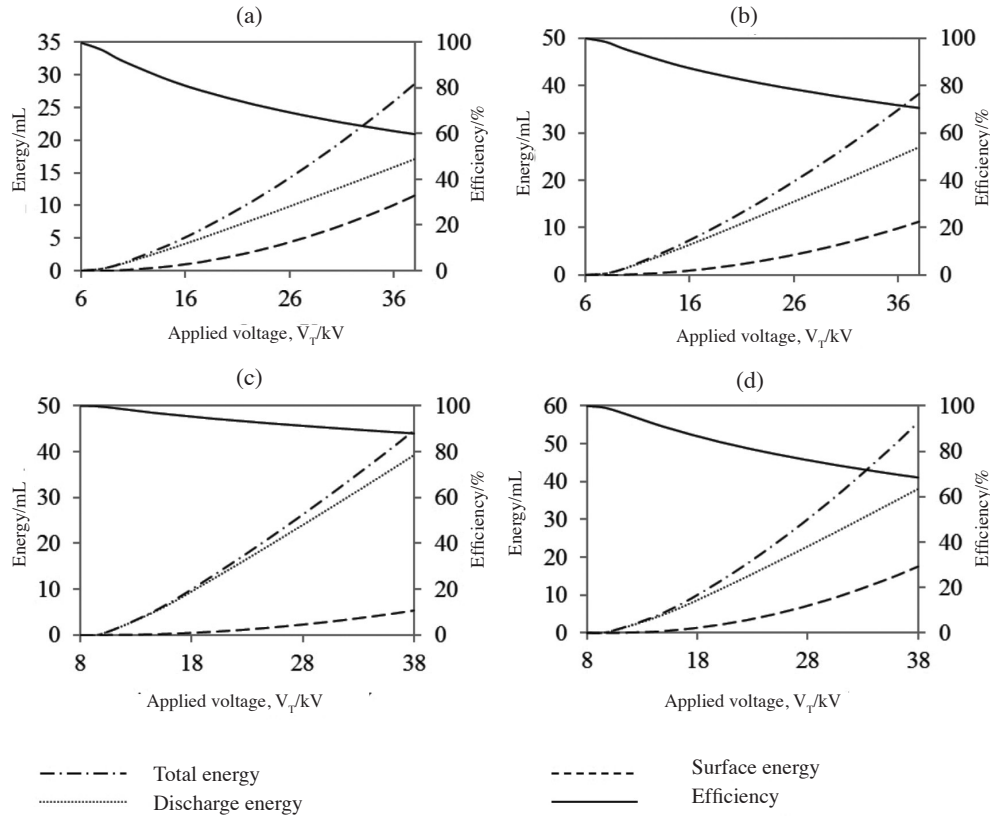
FIGURE 15. The graphs showing the simulated total energy, discharge energy, surface energy, and efficiency versus the applied voltage of smooth dielectric (a) 0.2 mm air gap, (b) 0.5 mm air gap and (c) 1.0 mm air gap. The rough dielectric with 1.0 mm air gap is shown in (d)

TABLE 1. A list of the simulation parameter

Glass plate	Space gap distance/ mm	Ratio, D	Surface resistance, $R_{sf}/M\Omega$	Dielectric capacitance, Cd/F	Space gap capacitance, Cg/F
Smooth surface	0.2	0.013	2.1	1.39E-10	1.42E-10
	0.5	0.014	2.3	1.39E-10	5.70E-11
	1.0	0.017	1.0	1.39E-10	2.85E-11
Rough surface	1.0	0.017	4.5	1.48E-10	2.85E-11

the DBD OFF period, charges remain on the dielectric surface and contributed to the memory effect. If the remaining charges recombined on the dielectric surface during the DBD OFF period, the QV diagram will reflect the change in total capacitance in the gradient of QV diagram.

The efficiency of the DBD in terms of the power dissipation at the DBD and due to the surface current has also been estimated from the simulation. The efficiency of the discharge with air gap 0.2, 0.5 and 1.0 mm at applied voltage of 10 to 35 kV are plotted in Figures 15(a), 15(b) and 15(c). Similar results for discharges using dielectric with rough surface are also plotted in Figure 15(c) for comparison. It is found that the efficiency reduces when the applied voltage is increased. For example, at 0.5 mm air gap efficiency of 94.6% at 10 kV reduced to 70.1% at 35 kV. This is because at higher applied voltage, more

energy is dissipated in the charge transfer process and on the dielectric surface as the excess voltage is higher.

CONCLUSION

The dynamic circuit model constructed and implemented using Matlab simulink has been shown to be able to simulate accurately the discharge characteristics of a 50 Hz filamentary discharge. The surface resistance that is introduced here represents the average effect that effectively sum the resistance encountered by the charges between the discharging and non-discharging regions on the surface of the dielectric. The values of surface resistance are also found to be dependent on the applied voltage and the thickness of the air gap. The surface resistance considered here comprises of the effect

due to the surface roughness of the dielectric layer, the trapping energy and the memory effect that in one way or another limit the mobility of the charges moving from the discharging region to the non-discharging region. In any case, the excess of energy due to the surface effect reflected in the expanded QV diagram has been reasonably well fitted and explained. This model will also be useful for DBD operated with non-conductive layer where charge accumulation on the localized regions is significant.

REFERENCES

Bartnikas, R., Radu, I. & Wertheimer, M.R. 2007. Dielectric electrode surface effects on atmospheric pressure glow discharges in helium. *IEEE Transactions on Plasma Science* 35: 1437-1447.

Bhosle, S., Zissis, G., Damelincourt, J.J., Capdevila, A., Gupta, K., Dawson, F.P. & Tarasenko, V.F. 2005. Electrical modeling of a homogeneous dielectric barrier discharge (DBD). *Conference Record of the 2005 IEEE Industry Applications Conference* 4: 2315-2319.

Bhosle, S., Zissis, G., Damelincourt, J.J. & Dawson, FP. 2004. Calculation of the impedance of an axisymetric DBD lamp for power supply design purposes. *Conference Record of the 2004 IEEE Industry Applications Conference* 3: 1667-1670.

Brandenburg, R., Navratil, Z., Jansky, J., St'ahel, P., Trunec, D. & Wagner, H.E. 2009. The transition between different modes of barrier discharges at atmospheric pressure. *Journal of Physics D-Applied Physics* 42(8): 085208.

Chirokov, A., Gutsol, A., Fridman, A., Sieber, K.D., Grace, J.M. & Robinson, K.S. 2006. A study of two-dimensional microdischarge pattern formation in dielectric barrier discharges. *Plasma Chemistry and Plasma Processing* 26: 127-135.

Falkenstein, Z. & Coogan, J.J. 1997. Microdischarge behaviour in the silent discharge of nitrogen-oxygen and water-air mixtures. *Journal of Physics D-Applied Physics* 30: 817-825.

Flores-Fuentes, A., Pena-Eguiluz, R., Lopez-Callejas, R., Mercado-Cabrera, A., Valencia-Alvarado, R., Barocio-Delgado, S. & de la Piedad-Beneitez, A. 2009. Electrical model of an atmospheric pressure dielectric barrier discharge cell. *IEEE Transactions on Plasma Science* 37(1): 128-134.

Gherardi, N. & Massines, F. 2001. Mechanisms controlling the transition from glow silent discharge to streamer discharge in nitrogen. *IEEE Transactions on Plasma Science* 29: 536-544.

Hashim, S.A., Wong, C.S., Abas, M.R. & Dahlan, K.Z. 2007. Feasibility study on the removal of nitric oxide (NO) in gas phase using dielectric barrier discharge reactor. *Malaysia Journal of Science* 26: 111-116.

Hashim, S.A., Wong, C.S., Abas, M.R. & Dahlan, K.Z. 2010. Discharge based processing systems for nitric oxide remediation. *Sains Malaysiana* 39: 981-987.

Kamchouchi, H.E. & Zaky, A.A. 1975. A direct method for the calculation of the edge capacitance of thick electrodes. *Journal of Physics D-Applied Physics* 8(2): 1365-1371.

Kim, G.H., Jeong, S.Y., Kwon, H.C. & Song, S.H. 2006. Capacitance between an atmospheric discharge plasma and the dielectric electrode in the parallel cell reactor. *Journal of the Korean Physical Society* 49: 1307-1311.

Kogelschatz, U., Eliasson, B. & Egli, W. 1997. Dielectric-barrier discharges. Principle and applications. *Journal De Physique Iv* 7: 47-66.

Kogelschatz, U., Eliasson, B. & Egli, W. 1999. From ozone generators to flat television screens: History and future potential of dielectric-barrier discharges. *Pure and Applied Chemistry* 71: 1819-1828.

Kogelschatz, U. 2002. Filamentary, patterned, and diffuse barrier discharges. *IEEE Transactions on Plasma Science* 30: 1400-1408.

Kogelschatz, U. 2003. Dielectric-barrier discharges: Their history, discharge physics, and industrial applications. *Plasma Chemistry and Plasma Processing* 23: 1-46.

Kozlov, K.V., Wagner, H.E., Brandenburg, R. & Michel, P. 2001. Spatio-temporally resolved spectroscopic diagnostics of the barrier discharge in air at atmospheric pressure. *Journal of Physics D-Applied Physics* 34: 3164-3176.

Li, M., Li, C.R., Zhan, H.M., Xu, J.B. & Wang, X.X. 2008. Effect of surface charge trapping on dielectric barrier discharge. *Applied Physics Letters* 92: 031503.

Liu, S.H. & Neiger, M. 2003. Electrical modelling of homogeneous dielectric barrier discharges under an arbitrary excitation voltage. *Journal of Physics D-Applied Physics* 36: 3144-3150.

Manley, T.C. 1943. The electric characteristics of the ozonator discharge. *Trans. Electrochem. Soc.* 84: 83-96.

Naude, N., Cambronne, J.P., Gherardi, N. & Massines, F. 2005. Electrical model and analysis of the transition from an atmospheric pressure Townsend discharge to a filamentary discharge. *Journal of Physics D-Applied Physics* 38: 530-538.

Pal, U.N., Sharma, A.K., Soni, J.S., Kr, S., Khatun, H., Kumar, M., Meena, B.L., Tyagi, M.S., Lee, B.J., Iberler, M., Jacoby, J. & Frank, K. 2009. Electrical modelling approach for discharge analysis of a coaxial DBD tube filled with argon. *Journal of Physics D-Applied Physics* 42(4): 045213.

Ramasamy, R.K., Rahman, N.A. & Wong, C.S. 2001. Effect of temperature on the ozonation of textile waste effluent. *Color Technol.* 117: 95-97.

Somerville, I. & Vidaud, P. 1985. Surface spreading of charge due to ohmic conduction. *Proceedings of the Royal Society of London Series a-Mathematical Physical and Engineering Sciences* 399: 277-293.

Subedi, D.P., Tyata, R.B., Khadgi, A. & Wong, C.S. 2012. Physiochemical and microbiological analysis of drinking water treated by using ozone. *Sains Malaysiana* 41: 739-745.

Valdivia-Barrientos, R., Pacheco-Sotelo, J., Pacheco-Pacheco, M., Benitez-Read, J.S. & Lopez-Callejas, R. 2006. Analysis and electrical modelling of a cylindrical DBD configuration at different operating frequencies. *Plasma Sources Science & Technology* 15: 237-245.

Wagner, H.E., Brandenburg, R., Kozlov, K.V., Sonnenfeld, A., Michel, P. & Behnke, J.F. 2003. The barrier discharge: Basic properties and applications to surface treatment. *Vacuum* 71: 417-436.

Plasma Technology Research Centre, Physics Department
University of Malaya
50603 Kuala Lumpur
Malaysia

*Corresponding author; email: cswong@um.edu.my